

The effects of ArUco marker velocity and size on motion capture detection and accuracy in the context of human body kinematics analysis


Bartosz Wieczorek

bartosz.wieczorek@put.poznan.pl |  <http://orcid.org/0000-0003-0808-298X>


Łukasz Warguła

lukasz.wargula@put.poznan.pl |  <http://orcid.org/0000-0002-3120-778X>


Mateusz Kukła

mateusz.kukla@put.poznan.pl |  <http://orcid.org/0000-0003-3456-3824>
Institute of Machine Design, Faculty of Mechanical Engineering, Poznan University of Technology

Arkadiusz Kubacki

arkadiusz.kubacki@put.poznan.pl |  <http://orcid.org/0000-0001-6353-5801>
Institute of Mechanical Technology, Faculty of Mechanical Engineering, Poznan University of Technology

Jan Górecki

jan.gorecki@put.poznan.pl |  <http://orcid.org/0000-0002-4640-7418>
Institute of Machine Design, Faculty of Mechanical Engineering, Poznan University of Technology

Scientific Editor: Andrzej Sobczyk, Cracow University of Technology Press
Technical Editor: Aleksandra Urzędowska, Cracow University of Technology Press
Language Editor: Tim Churcher, Big Picture
Typesetting: Anna Basista, Cracow University of Technology Press

Received: January 15, 2020
Accepted: November 2, 2020

Copyright: © 2020 Wieczorek, Warguła, Kukła, Kubacki, Górecki. This is an open access article distributed under the terms of the Creative Commons Attribution License, which permits unrestricted use, distribution, and reproduction in any medium, provided the original author and source are credited.

Data Availability Statement: All relevant data are within the paper and its Supporting Information files.

Competing interests: The authors have declared that no competing interests exist.

Citation: © 2020 Wieczorek B., Warguła Ł., Kukła M., Kubacki A., Górecki J., The effects of ArUco marker velocity and size on motion capture detection and accuracy in the context of human body kinematics analysis. *Technical Transactions*, e2020036. <https://doi.org/10.37705/TechTrans/e2020036>

Abstract

The research aim was to analyse the influence of velocity and size of markers on the accuracy of motion capture measurement utilising image processing with the use of OpenCV. On the basis of the obtained results, the usefulness of the applied measurement method in studying the kinematics of the human body while driving operating a wheelchair was determined. This article presents the test results for a low-budget motion capture measurement system for testing the kinematics of the human body in a single plane. The tested measuring system includes a standard activity camera Xiaomi Yi4K, expanded polystyrene markers with printed ArUco codes, and original software for marker position detection developed by the author. The analysis of the measurement method with regard to its applicability in biomechanical studies has highlighted several key factors: the number of measuring points, measurement accuracy expressed as a relative error and the limit velocity at which the marker trajectory is correctly represented. The article shows that the limit velocity of the marker is 2.2 m/s for 50x50 mm markers and 1.4 m/s for 30x30 mm markers. The number of measured points ranged from 233 to 2,457 depending on the marker velocity. The relative error did not exceed 5% for the marker velocities and thus provided a correct representation of its trajectory.

Keywords: velocity, applied measurement method, kinematics

1. Introduction

The measurement of human body kinematics is required in many different fields. In medicine, it supports orthopaedic diagnosis, verifies the progress of rehabilitation (Kopniak, 2014) and can be used to determine patterns, for example, in movement in healthy children, to create databases with comparative data (Kania, Głowacka-Kwiecień, 2008). It can also be used to evaluate angular changes in the joints of the lower limbs when walking with a knee orthosis restricting knee movement (Głodzik, Krężałek, Strój, Przybytek, Szczygieł, Hładki, 2017). In sports, it can support the development of proper technique (Kopniak, 2012), for example, testing athletes using rowing machines with motion acquisition systems, EMG systems, and heart rate monitors to develop the interdisciplinary procedures for the testing of rowers (Skublewska-Paszowska, Montusiewicz, Łukasik, Pszczoła-Pasierbiewicz, Baran, Smołka, Pueo, 2016). In psychology, it supports gesture analysis (Kopniak, 2012) or emotion analysis to allow for easy interpretation (Hachaj, Ogiela, Koptyra, 2018). For example, it can be used to detect behaviour based on motion recordings and detected behavioural patterns (Baran, 2018). In technical training, it can be used to evaluate the goals completed as part of simulation training, for example, in the case of the fire brigade during a simulated rescue mission (Kopniak, 2012). Yet another application covers remote control systems for robotic arms for the easy programming of industrial robot motion (Kamińska, Kopniak, Zysk, 2014) or tests in working conditions to determine the motion of, for example, drivers operating vehicles (Skublewska-Paszowska, Łukasik, Smołka, 2015). It can be used in the motion kinematics analysis in animals, including both linear and angular kinematics, e.g. horse movement analysis to predict sport event results, functional development and potential pathological conditions (Jóźwiak, Jaśkowski, Jóźwiak, Kosek, Knapkiewicz, Jakowski, 2014). Motion kinematics tests are used in many disciplines, as highlighted in the above examples. There are many methods and systems available to measure motion kinematics. They differ with regard to costs, measurement accuracy and their limited capabilities of being used in specific applications.

A review of the literature included methods used to determine the motion kinematics of the upper limbs during wheelchair propulsion, supporting the wheelchair design process by improving the ergonomics of the manual propulsion systems. Four Kinescan-IBV cameras and a wheelchair treadmill were used in the tests of athletes using wheelchairs. Time parameters were analysed and the upper limb kinematics were determined following ISP recommendations (Wu, van der Helm, Veeger, Makhsous, Van Roy, Anglin, Nagels, Karduna, McQuade, Wang, Werner, Buchholz, 2005). Time parameters for the motion phases, the points of contact between the hand and the wheel and the biological system angles were also recorded (Crespo-Ruiz, Del Ama-Espinosa, Gil-Agudo, 2011). The tests aimed to determine the arm loading during wheelchair propulsion using pushrim type and arm crank type propulsion were also tested. The kinematic data were collected using videos recorded at 100 Hz using a 6-camera image recording system (Oqus, Qualisys AB, Gothenburg, Sweden). The results were used to determine the position of the trunk and the left upper limb (Arnet, van Drongelen, Scheel-Sailer, van der Woude, Veeger, 2012). In the test, the patients manually propelled the pushrim and the lever on the wheelchair simulator at 3 km/h and 7.5 W/side (Watt per side). Three-dimensional measurements of the trunk, shoulder, elbow and wrist motion were recorded over durations of four seconds for each sitting position. The test aimed to determine the kinematic differences between the arm-crank and pushrim propulsion systems (Hughes, Weimar, Sheth, Brubaker, 1992). The test verified the effects of the used solution on the propulsion ergonomics and highlighted the need to analyse the upper limb motion trajectory to select a suitable technical configuration of for the wheelchair used (Hughes, Weimar, Sheth, Brubaker, 1992). The systems recording hand motion kinematics during wheelchair propulsion should provide motion recording at a rate of at least 2.13 m/s depending on the hand segment tested (Vanlandewijck, Theisen, Daly, 2001).

The review of the literature shows that motion kinematics studies use methods and equipment that require advanced markers, several cameras, and proprietary or commercially available data processing software. The article aims to carry out a methodological pilot study to analyse a low-budget motion capture system (Carse, Meadows, Bowers, Rowe, 2013) for use during human body kinematics testing in a single plane. The measuring system is an original prototype which includes a commonly available activity camera (in the used system case, it was the Xiaomi Yi4K camera), a set of plotter-cut 5-mm-thick EPS sheet markers and software developed by the author to detect the marker position based on the video recordings. The total cost of the measuring system with the software did not exceed 3,000 USD, which is less than other commercially available motion capture systems, including Vicon MX, Vicon 612 and Optitrack. The analysis of the measurement method regarding its applicability in biomechanical studies has highlighted several key factors: the number of measured points, measuring accuracy expressed as a relative error and the limit velocity at which the marker trajectory is correctly represented.

To summarise, the main goal of the conducted research focused on the measurement accuracy assessment of the marker position depending on its size and velocity. Before starting the study, a hypothesis was made that under certain kinematic conditions characteristic for operating driving a wheelchair, a low-cost measuring system can successfully match the advanced motion-capture systems already on the market. The analysed measurement accuracy focused on the accuracy assessment of the marker movement trajectory and the captured number of points.

2. Materials and methods

The test method is based on measuring the effect of the marker velocity and its size on the accuracy with which a known standard trajectory is represented. The trajectory was determined using a set of points collected during the visual detection of the ArUco marker using OpenCV libraries. A test stand comprising a standard wheel (1) with a diameter of $d = 530$ mm coupled with an electric motor (2) was used (Fig. 1). A fixed *IDO* marker was attached to the fixed wheel axle and an *ID1* marker was attached to the rotating standard wheel (1).

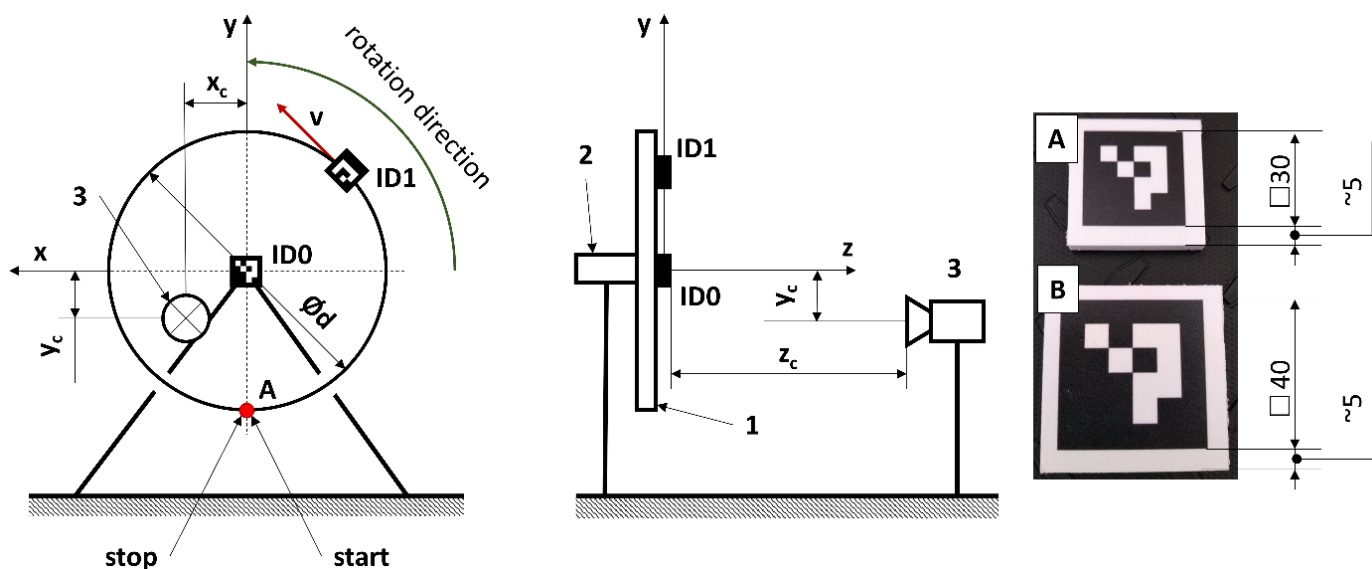


Fig. 1. Diagram of the test stand and ArUco markers: A – 30x30 marker, B – 40x40 marker, 1 – standard wheel, 2 – motor, 3 – camera, *IDO* – fixed marker, *ID1* – rotating marker, x_c – vertical offset of the camera lens in relation to *IDO* marker, y_c – horizontal offset of the camera lens in relation to *IDO* marker, z_c – distance between camera lens and *IDO* marker, d – standard wheel diameter, v – *ID1* marker linear velocity

The position of the markers was recorded using a camera (3) installed in such a way as to ensure a constant distance between the lens and the *ID0* marker. Two different markers were used in the test: a 30x30 mm marker (Fig. 1 A) and a 40x40 mm marker (Fig. 1 B). The coordinates defining the position of the camera lens in relation to the *ID0* marker were $x_c = \pm 10$ mm, $y_c = \pm 10$ mm, $z_c = 550 \pm 10$ mm. The video was recorded at 720 p/240 fps.

The tested video was recorded using a Xiaomi Yi4K camera, and each video included a complete turn of the *ID1* marker in relation to the *ID0* marker. Each rotation began and ended at point A (Fig. 1). The measurements were taken at the linear velocity of the marker from $v = 0.2$ m/s, which was increased by 0.2 m/s in the subsequent tests.

2.1. Measurement procedure

In accordance with the measurement procedure, the recorded video was processed using software developed by the author, in which the images of the *ID1* marker rotating in relation to the *ID0* marker were processed. The result was a file which included the coordinates of the position of the central point of the *ID1* marker.

The wheel radius was determined for each measured point based on the detection point of the *ID1* marker position. Using the total number of measured points n and the wheel radii, the mean wheel radius MR was determined for the ArUco markers detected in dynamic conditions. Using this value and a known standard wheel radius R to which the *ID1* marker was attached, a relative error (2) was determined for each linear velocity.

$$\text{Mean wheel radius: } MR = \sum_{i=1}^n \sqrt{x_i^2 + y_i^2} \quad (1)$$

$$\text{Relative error: } e = \frac{MR - R}{R} \cdot 100\% \quad (2)$$

where n is the number of measured points, x_i and y_i are the marker position coordinates on a plane parallel to the standard wheel, MR is the mean wheel radius determined based on the *ID1* marker detection, R is the standard wheel radius.

The idea behind the motion capture method is to represent the motion trajectory of the tested object. As a result, in addition to the relative error analysis, the number of measured points and their distribution at the standard wheel trajectory was also verified in the ArUco marker detection method. The analysis of point distribution consisted of dividing the standard wheel into four quadrants: $q1$, $q2$, $q3$ and $q4$ (3–6). Each quadrant was assigned a variability range for the *ID1* marker position coordinates. Based on these ranges, a percentage of all points in each quadrant was analysed. Based on qualitative evaluation, a 20% point distribution in a single quadrant was used. Any test showing the number of points in a single quadrant below this value was rejected.

$$q1: \begin{cases} x_i \in (-\infty; 0) \\ y_i \in (0; \infty) \end{cases} \quad (3)$$

$$q2: \begin{cases} x_i \in (0; \infty) \\ y_i \in (0; \infty) \end{cases} \quad (4)$$

$$q3: \begin{cases} x_i \in (0; \infty) \\ y_i \in (-\infty; 0) \end{cases} \quad (5)$$

$$q4: \begin{cases} x_i \in (-\infty; 0) \\ y_i \in (-\infty; 0) \end{cases} \quad (6)$$

3. Results

Video data processing involved imaging the distribution of the 30x30 *ID1* marker detection points 30x30 (Fig. 2) and the 40x40 *ID1* marker detection points (Fig. 3) in relation to the perimeter of the standard wheel. An analysis of the representation of the standard wheel with the *ID1* marker showed the threshold at which a circle is not represented by the detection points. For the 30x30 marker, the linear velocity limit of the *ID1* marker was $v = 1.6$ m/s, whereas for the 40x40 marker, the linear velocity limit was $v = 2.2$ m/s.

Based on the measured detection points, the central position of a circle was determined by calculating a mean value for all measured points. The coordinates of the centre position at $v = 0.2$ m/s are $x = 0.35$ mm and $y = -3.57$ mm for the 30x30 marker, and $x = -0.45$ mm and $y = -6.39$ mm for the 40x40 marker. At $v = 1.6$ m/s, the coordinates are $x = 8.10$ mm and $y = -23.38$ mm for the 30x30 marker. At $v = 2.2$ m/s, the coordinates are $x = 16.21$ mm and $y = -35.70$ mm for the 40x40 marker.

The results of the 30x30 marker detection re shown in Table 1 and the graphs representing the relative error, the number of measured points (Fig. 4) and the distribution of the detection points in each quarter (Fig. 5) are also presented. At $v = 0.20$ m/s, the program algorithm identified the marker 2,449 times in a single turn of the standard wheel. The relative error at this velocity was 0.48%, and the percentage distribution of the detection points in each quarter was between 24.62 and 25.81%. At a maximum velocity of $v = 1.6$ m/s yielding a correct representation of the standard trajectory, the algorithm identified the

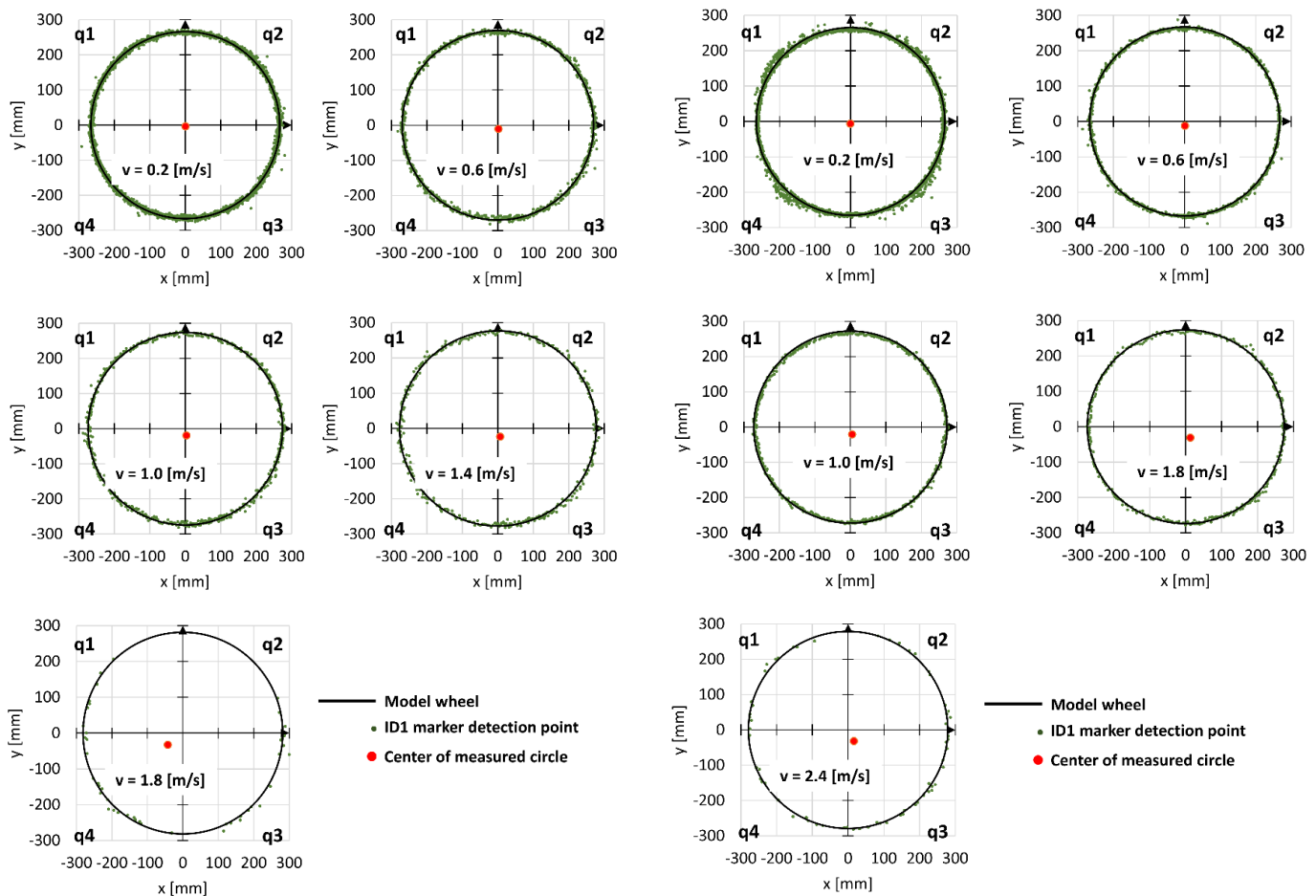


Fig. 2. Distribution of the 30x30 *ID1* marker detection points in relation to the outline of the standard wheel at different linear velocities v , q_1 , q_2 , q_3 , q_4 – standard wheel quarters

Fig. 3. Distribution of 40x40 *ID1* marker detection points in relation to the outline of the standard wheel for different linear velocities v , q_1 , q_2 , q_3 , q_4 – standard wheel quarters

marker 335 times in a single turn of the standard wheel. The relative error at this velocity was 4.44%, and the percentage distribution of the detection points in each quarter was between 22.52 and 32.13%.

Table 1. Detection points, mean circle radius MR , standard deviation of circle radius SDR , percentage distribution of the detection points in standard wheel quarters $q1$ – $q4$ and relative error for the 30x30 marker

Marker velocity	Number of detection points	MR	SDR	Points in $q1$	Points in $q2$	Points in $q3$	Points in $q4$	Relative error
[m/s]	[-]	[mm]	[mm]	[%]	[%]	[%]	[%]	[%]
0.20	2449.00	266.29	4.45	24.62	24.62	25.81	24.95	0.48
0.40	1238.00	267.99	4.72	24.47	24.31	26.82	24.39	1.13
0.60	839.00	269.93	4.93	24.08	23.84	27.77	24.31	1.86
0.80	642.00	271.55	4.59	23.52	23.52	28.97	23.99	2.47
1.00	521.00	274.10	5.11	23.42	23.03	29.56	23.99	3.43
1.20	437.00	275.80	4.95	23.34	22.65	30.66	23.34	4.08
1.40	379.00	277.14	5.77	22.96	22.43	31.40	23.22	4.58
1.60	335.00	276.77	22.13	22.82	22.52	32.13	22.52	4.44
1.80	282.00	280.61	6.20	31.21	14.18	29.43	25.18	5.89

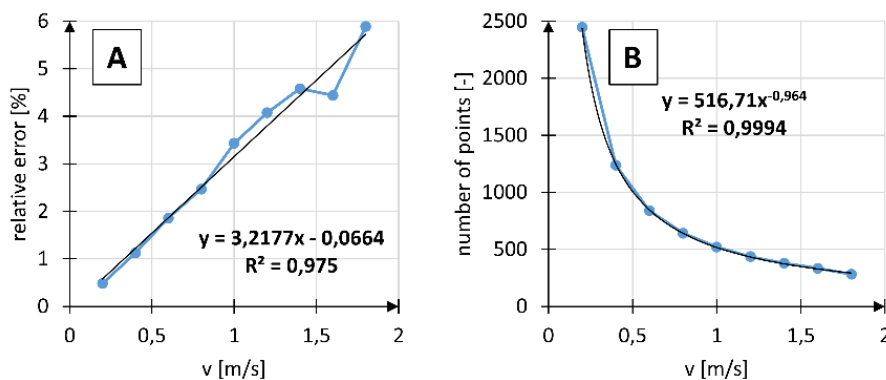


Fig. 4. Relative error (A) and the number of detection points (B) as a function of the 30x30 marker velocity

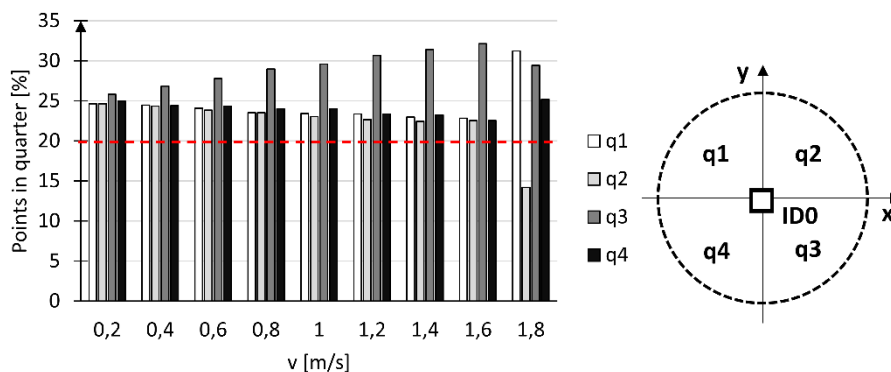


Fig. 5. Distribution of the detection points in each quarter of the standard wheel at various linear velocities of the 30x30 marker

Table 2 shows a summary of motion capture measurements for the 40x40 markers. The results are represented using graphs of the relative error, the number of measured points (Fig. 6) and the distribution of the detection points in each quarter (Fig. 7).

Table 2. Detection points, mean circle radius MR , standard deviation of circle radius SDR , percentage distribution of the detection points in standard wheel quarters $q1$ – $q4$ and relative error for the 40x40 marker

Marker velocity	Number of detection points	MR	SDR	Points in $q1$	Points in $q2$	Points in $q3$	Points in $q4$	Relative error
[m/s]	[-]	[mm]	[mm]	[%]	[%]	[%]	[%]	[%]
0.20	2457.00	265.13	5.86	24.66	24.30	26.09	24.95	0.05
0.40	1246.00	266.14	5.32	24.24	24.00	27.37	24.40	0.43
0.60	839.00	266.86	3.91	24.08	23.84	28.01	24.08	0.70
0.80	640.00	268.03	3.51	23.75	23.13	29.38	23.75	1.14
1.00	523.00	269.60	3.56	23.14	22.94	30.59	23.33	1.74
1.20	438.00	270.80	3.91	23.06	22.83	30.82	23.29	2.19
1.40	378.00	272.04	4.02	23.02	22.49	31.48	23.02	2.66
1.60	340.00	272.97	4.15	22.35	21.76	33.53	22.35	3.01
1.80	306.00	273.69	4.65	22.22	21.57	33.99	22.22	3.28
2.00	281.00	275.71	4.81	21.35	21.00	35.23	22.42	4.04
2.20	257.00	277.56	4.24	21.01	21.01	35.41	22.57	4.74
2.40	233.00	278.97	5.53	25.75	18.03	34.33	21.89	5.27

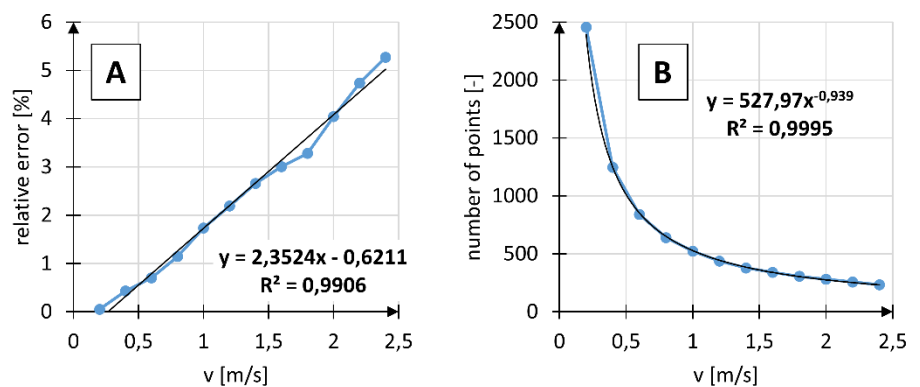


Fig. 6. Relative error (A) and the number of detection points (B) as a function of the 40x40 marker velocity

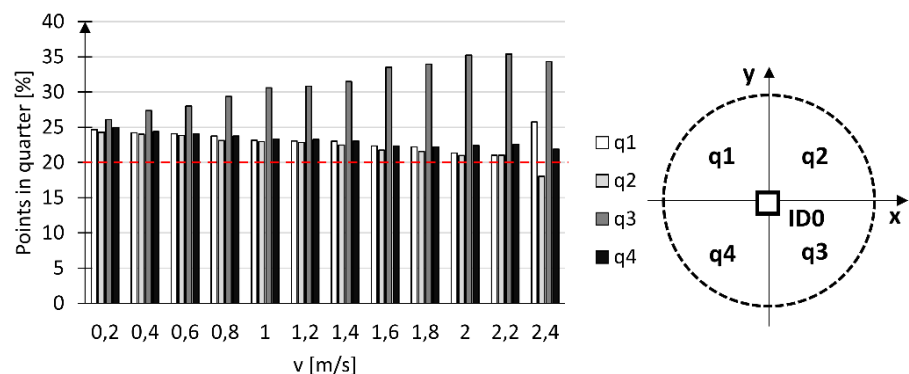


Fig. 7. Distribution of the detection points in each quarter of the standard wheel at various linear velocities of the 40x40 marker

At $v = 0.20$ m/s, the marker position was identified 2,457 times in a single turn of the standard wheel. The relative error at this velocity was 0.05%, and the percentage distribution of the detection points in each quarter was between 24.30 and 26.09%. At $v = 1.6$ m/s, the marker position was identified 340 times in a single turn of the standard wheel. The relative error at this velocity was

3.01%, and the percentage distribution of the detection points in each quarter was between 21.76 and 33.53%. At a maximum velocity of $v = 2.2$ m/s yielding a correct representation of the standard trajectory, the algorithm identified the marker 257 times in a single turn of the standard wheel. The relative error at this velocity was 4.74%, and the percentage distribution of the detection points in each quarter was between 21.01 and 35.41%.

4. Discussion

The analysis of the measurement method regarding its applicability in biomechanical studies has highlighted several key factors. The first is the recorded point number corresponding to the marker position at a given moment in time during the recording being analysed. The parameter depends on the video quality and the linear velocity of the marker. All videos were recorded at the same quality (720 p, 240 fps) with the linear velocity of the marker being the only variable. A comparison of the identified points for different marker sizes showed that the results are not affected by the marker size. At $v = 0.2$ m/s, 2,449 points were measured for the 30x30 marker, and 2,457 points were measured for the 40x40 marker. At $v = 1.2$ m/s, 437 points were measured for the 30x30 marker and 438 points were measured for the 40x40 marker. The detection of the marker position was affected only by its velocity. For both marker sizes, the number of measuring points as a function of the linear velocity of the marker can be expressed as a quadratic function.

The quality of the method can be defined by its accuracy, expressed as a relative error. The measured relative error indicates the percentage difference in the measured wheel radius in relation to the standard wheel radius. The analysis of the results shows that the measurement accuracy is affected by both the linear velocity and the size of the marker. At $v = 0.2$ m/s, the relative error was 0.48% for the 30x30 marker and 0.05% for the 40x40 marker. The relative error curve for subsequent linear marker velocities shows linearity. The marker size affects the error increase rate, i.e. the relative error function's slope depending on the linear velocity. The relative error at limit velocity $v = 1.6$ m/s was 4.44% for the 30x30 marker, and at $v = 2.2$ m/s, it was 4.74% for the 40x40 marker.

The applicability of the method in studies of motion kinematics of the human body is determined by the limit velocity at which the point motion trajectory is correctly represented. In the study, the occurrence of at least 20% of all measured marker detection points in each standard wheel quarter was used as a criterion for the correct representation of the trajectory. Based on this assumption, the limit velocity allowing the marker to be detected at 720 p/240 fps was 1.6 m/s for the 30x30 marker and 2.2 m/s for the 40x40 marker. A characteristic increase in the percentage of measured points in $q3$ for each measuring test was due to video processing. The processing method did not allow cutting of the section of the video representing a single turn of the wheel. As a result, the measured marker stayed slightly longer in the third quarter ($q3$) compared to the other quarters. The limit linear velocities of the marker are sufficient to test the human body kinematics during daily activities. For example, during wheelchair use, the shoulder and forearm velocities did not exceed the limit velocities (Chow, Chae, Crawford, 2000; Boninger, Cooper, Shimada, Rudy, 1998).

The verification confirmed the applicability of the ArUco marker detection method in the analysis of human body kinematics, in particular, the kinematics of manual wheelchair propulsion. In this case, due to the attachment point on the upper limb, the marker size should not exceed 40 mm to prevent restricting the movement. The tests also require uniform illumination of the marker without reflections. The recommended setup includes a set of 40 W incandescent light bulbs. To reduce the relative error and increase the range of linear marker velocities, the video quality and frame rate must be increased (Chow, Chae, Crawford, 2000; Boninger, Cooper, Shimada, Rudy, 1998). On the basis of the

carried out work, it was found that for the marker velocity greater than 2 m/s, the developed method is ineffective and does not allow determining the trajectory in such a way that may allow analysis of the entire marker movement. In addition, the marker size is a limitation, which translates into the measurement accuracy. In the case of markers greater than 40x40 mm, its velocity increases.

5. Conclusion

The presented research results describe a new kinematics measuring method for movement of the human body – for example, when driving a wheelchair – that does not require expensive and complicated motion capture systems. The added value to the state of the art is the marker velocity limit and its size parameters determination, at which the processed marker image detection points enable the kinematic analyses of biomechanical systems. Additionally, the conducted analysis enabled determination of the relative error characteristics and the number of measured points as a velocity function for two marker dimensions: 30x30 mm and 40x40 mm. The presented tests confirmed the usefulness of the method in the movement analysis of low velocity systems (not exceeding 2 m/s). The presented study shows a set of limit values for which the measurement with the described method is characterized by a low relative error.

References

- Arnet, U., van Drongelen, S., Scheel-Sailer, A., van der Woude, L.H., Veeger, D.H. (2012). Shoulder load during synchronous handcycling and handrim wheelchair propulsion in persons with paraplegia. *Journal of rehabilitation medicine*, 44(3), 222–228.
- Baran, K. (2018). Rozpoznawanie emocji za pomocą technologii: elektroencefalografia (EEG), motion capture i wirtualna rzeczywistość (VR). *Prace doktorantów Wydziału Elektrotechniki i Informatyki Politechniki Lubelskiej*, Wydawnictwo Politechniki Lubelskiej, Lublin 2018, 32–46.
- Boninger, M.L., Cooper, R.A., Shimada, S.D., Rudy T.E. (1998). Shoulder and elbow motion during two speeds of wheelchair propulsion: a description using a local coordinate system. *Spinal cord*, 36(6), 418–426.
- Carse, B., Meadows, B., Bowers, R., Rowe, P. (2013). Affordable clinical gait analysis: An assessment of the marker tracking accuracy of a new low-cost optical 3D motion analysis system. *Physiotherapy*, 99(4), 347–351.
- Chow, J.W., Chae, W.S., Crawford, M.J. (2000). Kinematic analysis of shot-putting performed by wheelchair athletes of different medical classes. *Journal of Sports Sciences*, 18(5), 321–330.
- Crespo-Ruiz, B.M., Del Ama-Espinosa, A.J., Gil-Agudo, Á.M. (2011). Relation between kinematic analysis of wheelchair propulsion and wheelchair functional basketball classification. *Adapted physical activity quarterly*, 28(2), 157–172.
- Głodzik, J., Krężałek, P., Strój, E., Przybytek, M., Szczygieł, E., Hładki, W. (2017). Ocena zaburzeń chodu z wykorzystaniem analizy komputerowej BTS-SMART. *Ostry Dyżur*, 10(4).
- Hachaj, T., Ogiela, M.R., Koptyra, K. (2018). Human actions recognition from motion capture recordings using signal resampling and pattern recognition methods. *Annals of Operations Research*, 265(2), 223–239.
- Hughes, C.J., Weimar, W.H., Sheth, P.N., Brubaker, C.E. (1992). Biomechanics of wheelchair propulsion as a function of seat position and user-to-chair interface. *Archives of physical medicine and rehabilitation*, 73(3), 263–269.
- Józwiak, P., Jaśkowski, B.M., Józwiak, A., Kosek, W., Knapkiewicz, P., Jakowski, J.M. (2014). Kinematyczna ocena ruchu konia. *Med. Weter*, 70(1), 30–35.

- Kamiński, M., Kopniak, P., Zyla, K. (2014). Zdalne sterowanie ramieniem robota z wykorzystaniem inercyjnych czujników rejestracji ruchu. *Logistyka*, 6, 5168–5177.
- Kania, E., Głowacka-Kwiecień, A., Jochymczyk, K., Jureczko, P. (2008). Badania doświadczalne chodu dzieci zdrowych. *Aktualne Problemy Biomechaniki*, 2.
- Kopniak, P. (2012). Rejestracja ruchu za pomocą urządzenia Microsoft Kinect. *Pomiary Automatyka Kontrola*, 58(11), 1016–1018.
- Kopniak, P. (2014). Pomiary kątów ugięcia kończyny w stawie z wykorzystaniem inercyjnego systemu Motion Capture. *Pomiary Automatyka Kontrola*, 60(8).
- Skublewska-Paszowska, M., Łukasik, E., Smółka, J. (2015). Wykorzystanie systemu akwizycji ruchu do badania kierowców. *Logistyka*, 4, 5678–5684.
- Skublewska-Paszowska, M., Montusiewicz, J., Łukasik, E., Pszczoła-Pasierbiewicz, I., Baran, K.R., Smółka, J., Pueo, B. (2016). Motion capture as a modern technology for analysing ergometer rowing. *Advances in Science and Technology Research Journal*, 10(29).
- Vanlandewijck, Y., Theisen, D., Daly, D. (2001). Wheelchair propulsion biomechanics. *Sports medicine*, 31(5), 339–367.
- Wu, G., van der Helm, F.C.T., Veeger, H.E.J., Makhsous, M., Van Roy, P., Anglin, C., Nagels, J., Karduna, A.R., McQuade, K., Wang, X., Werner, F.W., Buchholz, B. (2005). ISB recommendation on definitions of joint coordinate systems of various joints for the reporting of human joint motion—Part II: Shoulder, elbow, wrist and hand. *Journal of Biomechanics*, 38, 981–992.